frontiers | Frontiers in Materials

TYPE Original Research
PUBLISHED 28 November 2025
DOI 10.3389/fmats.2025.1704881

OPEN ACCESS

EDITED BY
Riyadh Al-Raoush,
Qatar University, Qatar

REVIEWED BY
Pavlo Maruschak,
Ternopil Ivan Pului National Technical University, Ukraine
Bohan Yang,
Northeastern University, China
Tugrul Kasap,
Recep Tayyip Erdoğan University, Türkiye

*CORRESPONDENCE
Lei Wang,
wangleilei@jxust.edu.cn
Liping Zuo,
780374986@qq.com

RECEIVED 14 September 2025
REVISED 16 November 2025
ACCEPTED 17 November 2025
PUBLISHED 28 November 2025

CITATION
Liu R, Wang L, Xu S, Zhu D and Zuo L (2025) Microstructure and mechanical behavior of lithium slag-quartz sand cemented backfill: influence of particle gradation and content. *Front. Mater.* 12:1704881.
doi: 10.3389/fmats.2025.1704881

Microstructure and mechanical behavior of lithium slag-quartz sand cemented backfill: influence of particle gradation and content

Rongxi Liu[1], Lei Wang[1,2]*, Sidong Xu[1], Daopei Zhu[1] and Liping Zuo[1]*

[1]School of Civil Engineering and Surveying and Mapping Engineering (Nanchang), Jiangxi University of Science and Technology, Nanchang, China, [2]School of Software Engineering, Jiangxi University of Science and Technology, Nanchang, China

To achieve the sustainable development of industrial solid waste resource utilization and mining environmental remediation, this study investigates the mechanical properties and microstructure of cemented backfill (LQCB) prepared from lithium slag (LS) and quartz sand (QS) under different mix proportions. Through uniaxial compressive strength (UCS) tests, stress-strain analysis, and scanning electron microscopy (SEM) observation, the effects of QS content (10%–50%), particle size (1–8 mm), and cement-to-liquid ratio (C/Ls = 1:2, 1:4, 1:6) were systematically evaluated. The results show that when the QS content is 30%, particle size is 1–2 mm, and C/Ls is 1:2, the LQCB achieves optimal strength and compactness, with a UCS of 0.77 MPa and a minimum crack width of 15 μm. A higher QS content (≥50%) or excessively coarse particles increase porosity and weaken the interfacial transition zone, leading to a maximum UCS reduction of 63%. However, when the QS content is maintained at 30% with a particle size of 4–8 mm, the LQCB exhibits a maximum UCS of 1.07 MPa. SEM analysis confirms that the uniform distribution of hydration products (C-S-H and AFt) improves the microstructural integrity, while excessive QS results in widened cracks (up to 94.7 μm) and strength loss. The findings provide valuable guidance for optimizing the LQCB mix proportion, enhancing its performance, and promoting the reuse of solid waste.

KEYWORDS

lithium slag, quartz sand, lithium slag-quartz sand cemented backfill, mechanical properties, microstructure, interfacial transition zone

1 Introduction

As global resource extraction and energy production continue to expand, the generation of solid waste from mining and industrial activities has been increasing annually. These solid wastes not only consume significant land resources but also pose serious environmental threats, including heavy metal pollution (Kolandhasamy et al., 2024), soil acidification (Wei et al., 2023), and ecological damage (Nongthombam et al., 2024). As a result, the resource recovery and utilization of solid waste have become a major research focus in both academic and industrial fields (Wu et al., 2022; Lu et al., 2023; Li N. et al., 2024). Within

mine backfilling technology, the reuse of industrial solid waste offers a practical approach to managing waste storage while also enhancing surface subsidence control and ensuring underground safety during mining operations (Zhu et al., 2023; Ma et al., 2023). With the continuous development and utilization of lithium resources, lithium slag, as an industrial solid waste generated during lithium ore extraction or lithium salt production, is rapidly accumulating. If improperly disposed of, it will cause significant harm in three dimensions: environmental damage, human health hazards, and engineering performance deterioration. Therefore, the research and optimization of lithium slag backfilling technology is a new development direction.

Significant advancements have been made in the study of cemented backfill in recent years, particularly regarding the utilization of tailings, waste rock, and industrial solid waste as aggregates or cementitious materials, providing valuable theoretical insights for backfill design and application. Li M. et al. (2022) investigated the impact of waste rock particle size distribution on backfill properties, finding that continuous gradation with a higher fine particle fraction significantly enhanced backfill density and strength. Similarly, Wang Y. et al. (2022) investigated the impact of aggregate size distribution, fractal dimension, and confining pressure on cemented coal gangue backfill materials. Their experimental analysis revealed correlations between these parameters and mechanical properties, such as compressive strength and elastic modulus, while also establishing the optimal fractal dimension range and developing a model to predict mechanical properties, thereby further advancing the theoretical link between fractal dimension and mechanical behavior. Concerning dynamic mechanical properties, Cao et al. (2020) prepared CTC (Cemented Tailings Composite) specimens under specific parameters and subjected them to Split Hopkinson Pressure Bar impact loading combined with SEM analysis. The results demonstrated that the dynamic compressive strength increased exponentially with the average strain rate, and variations in the strain rate influenced the failure mode, guiding the reduction of underground mining dilution. Likewise, Lyu et al. (2023) investigated the impact of the Talbot gradation index on backfill mechanical behavior, finding that a Talbot index of 0.5 yielded the highest dynamic peak compressive strength, minimal energy dissipation, and maximum energy transfer efficiency. Furthermore, P.D. et al. investigated the impact fracture mechanisms of epoxy composites reinforced with silicon carbide particles at varying concentrations. The findings revealed that the inhomogeneity of epoxy composites at different structural scales significantly affects their physical and mechanical properties (Stukhlyak et al., 2015).

Regarding cementitious material substitution, Li H. et al. (2024) investigated the feasibility of using coal slag to replace cementitious materials partially and found that when the replacement ratio was 20%, the compressive strength of the backfill improved while the overall material cost significantly decreased, highlighting the economic value and engineering applicability of industrial by-products in backfill materials. Additionally, Chen et al. (2020) demonstrated through experiments that when the coarse particle content reached 50%, the specimen's UCS reached a peak of 0.687 MPa. Wang et al. (2020a) tested the compressive strength behavior and acoustic emission characteristics of cemented backfill under different water-cement ratios and height ratios. The results showed that the compressive strength decreased with an increase in the h/H (height of middle layer (h) to the whole height (H)) ratio and a decrease in the c/t (Cement-tailings) ratio, with the failure mode transitioning from tensile failure to a combined tensile-shear failure. Overall, the above literature systematically analyzed the optimization methods of cemented backfill in terms of particle size distribution, dynamic performance, and cementitious material substitution, proposing innovative theoretical models and experimental data with high reference value. These research findings have significantly contributed to revealing the internal mechanical properties and microstructural behavior of backfill, laying a solid theoretical foundation for performance improvement and multi-component optimization (Zhu et al., 2025; Liu et al., 2023). However, most current studies focus on the impact of a single factor on the performance of cemented backfill, while systematic research on the crack propagation law and material optimization mechanism under the coupling effect of multiple factors is insufficient. (Wang J. et al., 2022; Song et al., 2022). Meanwhile, most existing studies take tailings and coal gangue as the main aggregates, while the exploration on the synergistic mechanism between lithium residue (an active cementitious material) and quartz sand (a high-strength aggregate) remains insufficient. The QLCRB (Quartz Sand-Lithium Slag Cemented Rock Backfill) demonstrated significant potential for application in mine backfilling due to its unique material properties and environmental advantages. Lithium slag, as an active cementitious material, can generate C-S-H gel and ettringite through hydration reactions, contributing to structural reinforcement (Hellmers et al., 2025; Dong et al., 2025; Dong et al., 2024). Quartz sand, as a high-strength aggregate, offers excellent particle interlocking and void-filling capabilities (Yang et al., 2025; Ji et al., 2024; Antonovič et al., 2022).

Combining the two materials for mine backfilling not only enables the resource utilization of lithium slag and mitigates its environmental impact but also enhances the safety and stability of mine backfill by optimizing mechanical properties. Therefore, investigating the synergistic interaction mechanism between lithium slag and quartz sand in cemented backfill and exploring the optimization of their mechanical properties and microstructure is crucial for advancing green mining and sustainable resource development. The mechanical properties and microstructure must comply with the standards ASTM C0039_C0039M-24 and DANSK DS/EN ISO 14918. In this study, the effects of quartz sand content (10%–50%), particle size (1–8 mm) and cement-lithium slag ratio (C/LS = 1:2, 1:4, 1:6) on the mechanical properties and microstructure of LQCB were systematically explored by uniaxial compressive strength (UCS) test, stress-strain analysis, scanning electron microscopy (SEM) and energy spectroscopy (EDS) characterization, and the coupling law of the three was clarified. It is expected to reveal the correlation mechanism between the distribution of hydration products (C-S-H, AFt), the characteristics of the interfacial transition zone (ITZ) and macroscopic strength, which will provide a scientific basis for the optimization of the ratio of lithium slag-quartz sand cemented backfill, and promote the resource utilization of industrial solid waste and the development of green mining technology.

This study provides a comprehensive investigation of the synergistic lithium slag-quartz sand system for mine backfilling applications, establishing a new understanding of how these

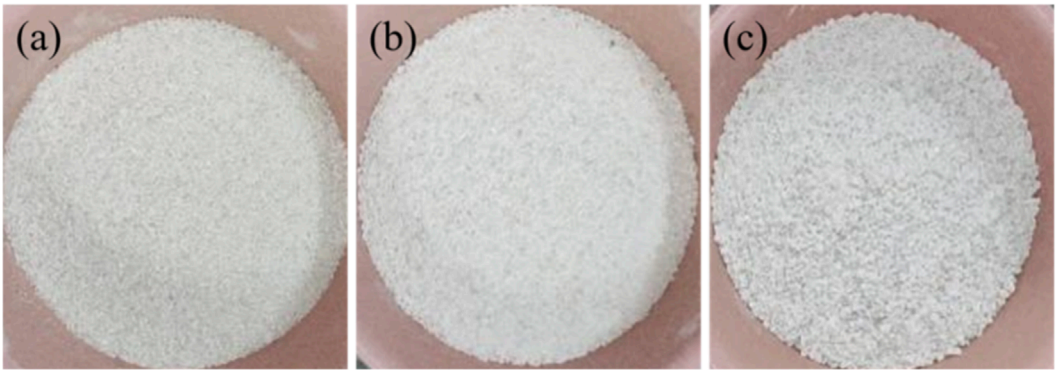

FIGURE 1
The quartz sand employed in this study was classified into the following size ranges: **(a)** 1–2 mm, **(b)** 2–4 mm, **(c)** 4–8 mm.

industrial byproducts interact at both macro and micro scales. Through systematic experimentation and characterization, we reveal fundamental relationships between particle size distribution, interfacial bonding characteristics, and mechanical performance that have not been previously reported for this material combination. The work advances the field by quantitatively linking microstructural evolution, particularly hydration product formation and crack propagation patterns, with the engineering properties of these sustainable backfill composites, while providing practical guidelines for optimizing waste utilization in mining applications. These findings provide both scientific insights into the behavior of composite materials and actionable solutions for developing more effective and environmentally responsible backfill technologies.

2 Test materials and methods

2.1 Materials

2.1.1 Quartz sand

In this study, quartz sand produced in Henan Province was selected as the aggregate, as shown in Figure 1. Its primary component is silicon dioxide, characterized by a uniform particle size and strong chemical inertness. According to the experimental design, the quartz sand particles were classified into three size ranges: 1–2 mm, 2–4 mm, and 4–8 mm. The quartz sand was mechanically sieved and stored in a dry, sealed environment. During specimen preparation, the material contributed to structural support and particle interlocking. Quartz sand has a specific gravity of 2.61–2.67, with specific surface areas ranging from 0.3–1.0 m^2/g (1–2 mm), 0.15–0.5 m^2/g (2–4 mm), and 0.08–0.3 m^2/g (4–8 mm). The particle density is 2.60–2.66 g/cm^3.

2.1.2 Cement, lithium slag, and water

Ordinary Portland Cement (OPC 42.5R) was used as the cementitious material in this study, known for its good early strength and long-term durability. Lithium slag, a by-product derived from the refining of spodumene, mainly consists of fine particles (Yuan et al., 2024). To ensure the accuracy of the test results, lithium slag was dried in a DGG-9240 electric furnace at 100 °C for 12 h prior to the experiment,the dried lithium slag was then ground into fine particles using a ball mill. The specific gravity of lithium slag is 2.4–2.8, the specific surface area is about 400 m^2/kg, and the particle density is 2.4–2.8 g/cm.Municipal tap water was used as the mixing water in the experiment for the homogeneous blending of lithium slag, cement, and quartz sand. The chemical composition of the municipal water met drinking water standards and required no further treatment. The water-to-binder ratio was strictly controlled during the experiment to ensure consistency of the specimens. To ensure experimental consistency, all quartz sand, cement, and lithium slag specimens were stored in sealed containers to prevent moisture absorption or chemical alterations.

To fully understand the properties of the raw materials, X-ray fluorescence spectroscopy (XRF) was used to analyze the primary chemical composition of lithium slag and quartz sand. The XRF analysis parameters were set to a scanning speed of 300/min, a voltage of 60 kV, and a current of 140 mA. The results are shown in Table 1. Additionally, a laser particle size analyzer was used to measure the particle size distribution of the lithium slag, as shown in Figure 2.

2.2 Experimental techniques

Cement and lithium slag were used as the primary cementitious materials in this study, with cement/lithium slag (C/Ls) ratios of 1:2, 1:4, and 1:6 in Table 2, to investigate their influence on the properties of the backfill material. The control group consisted of lithium slag-cement composites without quartz sand (0% QS content) in Table 3, with the same composition as the experimental group, to evaluate the impact of QS addition on backfill performance (The performance of the control group in the following text was 1:6). A solid content of 72 wt% was used to prepare the backfill mixtures, which were then cured for 7 days (By leveraging the reactive gelation properties of lithium slag, low C/LS ratios (e.g., 1:6) enhance solid waste utilization efficiency while high C/LS ratios (e.g., 1:2) ensure structural integrity. This ratio range addresses both “cost-effectiveness” and “high-strength requirements” in engineering applications. Preliminary experiments

TABLE 1 Primary chemical composition of lithium slag and quartz sand.

Materials	SiO_2	Al_2O_3	Fe_2O_3	CaO	MgO	Na_2O	K_2O	SO_3	H_2O	TiO_2	Loss on ignition (LOI)
LS	39.8	15.3	3.98	16.9	1.4	0.717	0.783	20.4	-	-	-
QS	99.83	0.05	0.01	0.003	0.002	0.012	0.013			0.012	0.03

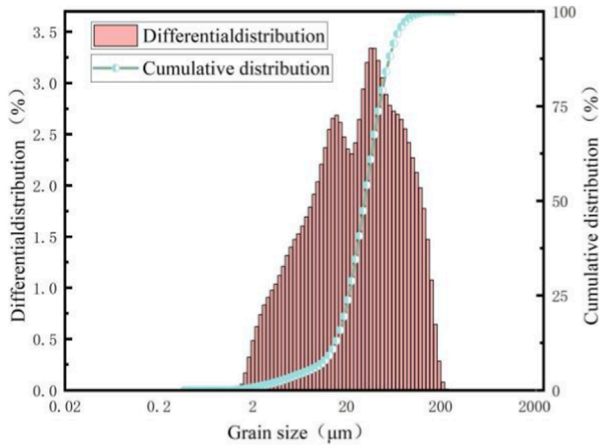

FIGURE 2
The particle size distribution of lithium slag.

revealed that slurry water separation becomes severe when solid content drops below 72%, while exceeding 72% hinders uniform mixing. When QS content surpasses 50%, hydration products fail to fully encapsulate aggregates, causing a dramatic strength drop. The LQCB formulation completes primary hydration reactions within 7 days, stabilizing strength and effectively demonstrating how mix design variations influence performance). All raw materials, including cement, lithium slag, quartz sand, and municipal water, were precisely measured before preparation. The weighing was conducted using a YHC 60001 electronic balance with a precision of 0.01 g, ensuring consistency and accuracy in the experiment. During preparation, pre-weighed lithium slag, cement, quartz sand, and water were added sequentially to the mixing container in accordance with the designed ratios, and the mixture was then thoroughly mixed. The mixing duration was maintained for at least 3 min to ensure homogeneous dispersion and complete blending of the slurry. The well-mixed slurry was then poured into a pre-lubricated standard cylindrical mold (50 mm in diameter and 100 mm in height). The inner surface of the mold was coated with a release agent to facilitate subsequent demolding. Upon filling, the mold was transferred into a SHBY-40 B fixed temperature/humidity curing chamber, maintained at a constant temperature of 22 °C ± 2 °C and 92% ± 2% relative humidity for curing. After an initial curing period of 24 h, the specimens were demolded and further cured under the same conditions until the target curing duration (7 days) was reached. Figure 3 presents the main steps involved in specimen preparation, covering material weighing, mixing, casting, curing, and demolding.

2.3 Uniaxial compressive strength test

To assess the mechanical performance of specimens with varying mix ratios, the uniaxial compressive strength (UCS) tests were performed on LQCB specimens. Test standard is ASTM C0039_C0039M-24. Before testing, each cylindrical specimen was precisely polished using a grinding device to ensure that the flatness of both ends met the experimental requirements. A precision measuring tool was then used to record the flatness data. The UCS test was performed using a WDWI-100 uniaxial compression testing machine with a loading rate of 0.5 mm/min. During the entire testing process, the machine continuously recorded load-displacement data in real-time using a computerized system to ensure data accuracy and completeness. In order to improve the reliability and representativeness of the experimental results, three samples were prepared for each mixing proportion, and the average UCS was calculated according to the test results. If the difference between the maximum and minimum UCS of the three samples was more than 3%, three samples were prepared again for the experiment.

2.4 SEM microscopic images

To investigate the internal microstructure and hydration products of the backfill samples in detail, a Zeiss Evo 18 scanning electron microscope (SEM) was used for characterization. The SEM was used to observe the morphology of hydration products, the distribution characteristics of microcracks, and the microstructure of the ITZ between the matrix and aggregates, exploring their relationship with material performance. Before testing, the specimens were thoroughly dried to eliminate any residual moisture. Subsequently, the sample surfaces were vacuum-coated and subjected to two rounds of carbon spraying to enhance surface conductivity and prevent charging effects. The SEM analysis parameters were as follows: an accelerating voltage range of 3–5 kV, a maximum magnification of ×2000, and a resolution of 3 nm, ensuring a clear observation of the sample microstructure.

3 Results and discussion

3.1 Effect of quartz sand content on the strength properties of backfill

The experimental results from the UCS test show that the compressive strength of LQCB specimens is significantly influenced by the cement-to-lithium slag (C/LS), quartz sand content, and sand particle size. In Figure 4a, the UCS of the lithium slag-quartz

TABLE 2 Backfill material mix.

Cement/Lithium slag (C/Ls) ratios	QS content (%)	Cement(g)	Lithium slag(g)	Water (ml)	Quartz sand (g)
1–2	10	302.4	604.8	392	100.8
1–4		181.44	725.76	392	100.8
1–6		129.6	777.6	392	100.8
1–2	20	268.8	537.6	392	201.6
1–4		161.28	645.12	392	201.6
1–6		115.2	691.2	392	201.6
1–2	30	235.2	470.4	392	302.4
1–4		141.12	564.48	392	302.4
1–6		100.8	604.8	392	302.4
1–2	40	201.6	403.2	392	403.2
1–4		120.96	483.84	392	403.2
1–6		86.4	518.4	392	403.2
1–2	50	168	336	392	504
1–4		100.8	403.2	392	504
1–6		72	432	392	504

TABLE 3 Control group backfill mix ratio.

Cement/Lithium slag (C/Ls) ratios	QS content (%)	Cement(g)	Lithium slag(g)	Water (ml)	Quartz sand (g)
1–2	0	336	672	392	0
1–4		201.6	806.4	392	0
1–6		144	864	392	0

sand cemented backfill specimens at C/Ls ratios of 1:2, 1:4, and 1:6 was 3 MPa, 2.22 MPa, and 1.66 MPa, respectively, indicating a significant decrease in strength as the C/Ls ratio decreased. Under all C/LS ratios, increased QS content consistently reduces UCS, with the most significant effect observed at C/LS = 1:6. This ratio is therefore highlighted for demonstrating the particle size-content coupling effect. Additionally, the experimental results show that the compressive strength of the lithium slag-quartz sand cemented backfill is negatively correlated with the quartz sand content, as shown in Figure 4b. As the quartz sand content increased from 10% to 50%, the strength decreased significantly, from 1.19 MPa to 0.44 MPa, representing a 36.97% decrease. The main reason for this phenomenon was that the strength of the backfill mainly relied on the hydration products of the cement slurry (such as CSH gel and Ca $(OH)_2$) formation (Zhang H. et al., 2023; Guo et al., 2018). As the quartz sand content increased, more quartz sand particles needed to be encapsulated by the cement slurry; however, the relative content of the cement slurry decreased, which prevented the formation of sufficient cementation. The coverage of quartz sand particles by the cement slurry became insufficient, forming more weak areas are formed in the backfill layer. Additionally, as the quartz sand content increased from 10% to 50%,The proportion of the interfacial transition zone (ITZ) between the quartz sand aggregate and the hydrated product cementitious matrix increases significantly (Shi et al., 2020), and these regions generally have lower strength and cannot effectively transmit and distribute stress, thereby reducing compressive strength (Sari et al., 2023).

At the same time, the particle size analysis further demonstrates the impact of quartz sand particle size on strength. Figure 4c shows that with quartz sand of a particle size of 2–4 mm, the specimen exhibited a trend where strength decreases as the quartz sand content increased, from 0.76 MPa to 0.42 MPa. A similar trend was

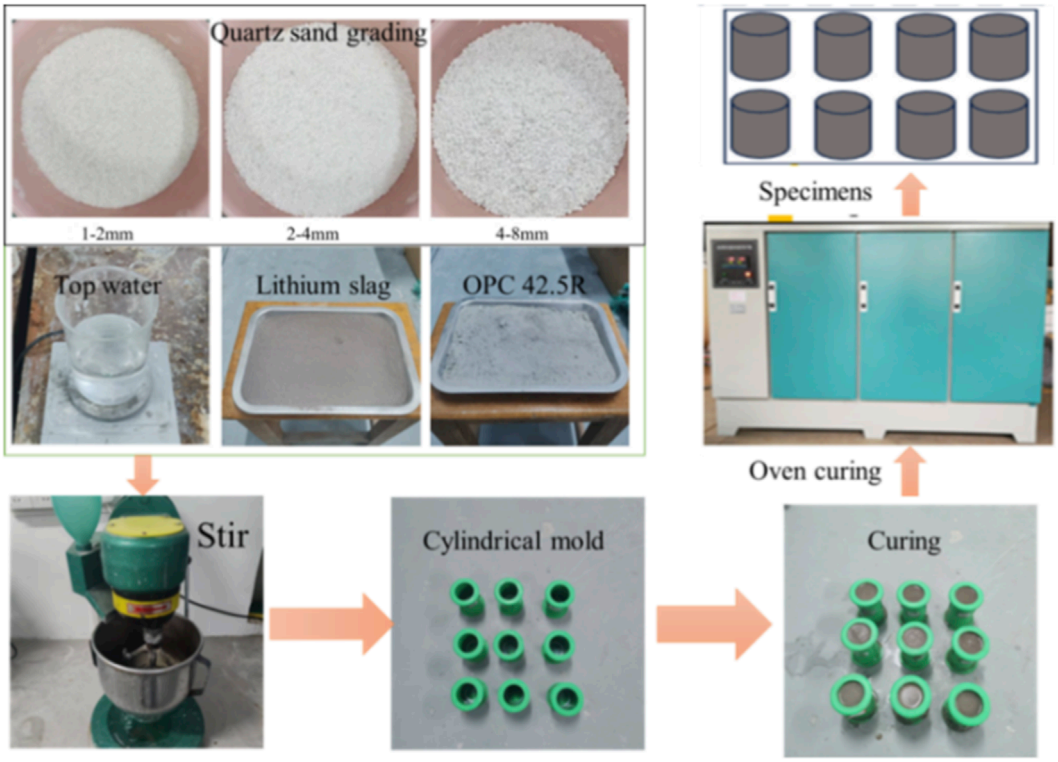

FIGURE 3
The preparation process of LQCB specimens.

confirmed under the condition of quartz sand with a particle size of 4–8 mm, as shown in Figure 4d, where the strength of the specimen decreased to 0.52 MPa. This indicates that quartz sand with a larger particle size significantly reduced the compactness and cementation effect of the backfill, leading to a reduction in strength to its lowest value (Xin et al., 2022; Zhou et al., 2020).

In general, in the initial phase of the effect of quartz sand content on specimen strength, excessive quartz sand content caused the internal structure of the specimen to become loose due to the limited cementation ability of the cement slurry. The cement slurry cannot completely encapsulate the quartz sand particles, leaving the pores partially unfilled, which results in a decrease in strength. When the quartz sand content was moderate, a relatively stable interlocking structure formed between the particles, filling the pores under the cementation effect of the cement slurry and providing the specimen with a certain strength. However, as the quartz sand content increased further, particularly when the proportion of fine particle-size quartz sand was too high, the number of interface transition zones in the specimen increased, and the cementing material was insufficient to support the overall structure, leading to a significant reduction in compressive strength.

In conclusion, there exists a significant negative correlation between quartz sand content and backfill compressive strength. When the quartz sand content exceeds 50%, insufficient cementitious materials lead to increased interfacial transition zones and higher porosity, resulting in a maximum 63% reduction in strength. Conversely, a suitable 30% content achieves optimal structural density and bonding efficiency through particle interlocking effects. This finding provides a practical guideline for determining appropriate quartz sand proportions in mine backfill projects, balancing solid waste utilization efficiency with structural safety requirements.

3.2 Effect of quartz sand gradation on the strength of the backfill

Figure 5 illustrates how quartz sand content affects the UCS of the lithium slag-quartz sand cemented backfill. Overall, as the quartz sand content increased, the UCS value gradually decreased, and the UCS value of LQCB samples was lower than that of the control group. At lower quartz sand contents, the decrease in strength was more pronounced. When the quartz sand content was 10%, the UCS decreased from 1.58 MPa to 0.76 MPa, a decrease of 0.82 MPa; When the quartz sand content was 20%, the UCS decreased from 1.31 MPa to 0.71 MPa, a reduction of 0.6 MPa; As the quartz sand content increased to 30%, the rate of decrease slowed down, with UCS dropping from 1.07 MPa to 0.66 MPa, a decrease of 0.41 MPa. When the quartz sand content was 40%, the UCS decreased from 0.65 MPa to 0.53 MPa, a reduction of 0.12 MPa; When the quartz sand content reached 50%, the UCS further decreased from 0.52 MPa to 0.42 MPa, a reduction of 0.1 MPa. This indicates that the increase in quartz sand grading and content leads to a higher porosity, weakening of the interface transition zone, and insufficient coverage of hydration products (Kasap et al., 2022), which significantly weakens the compressive strength of the backfill

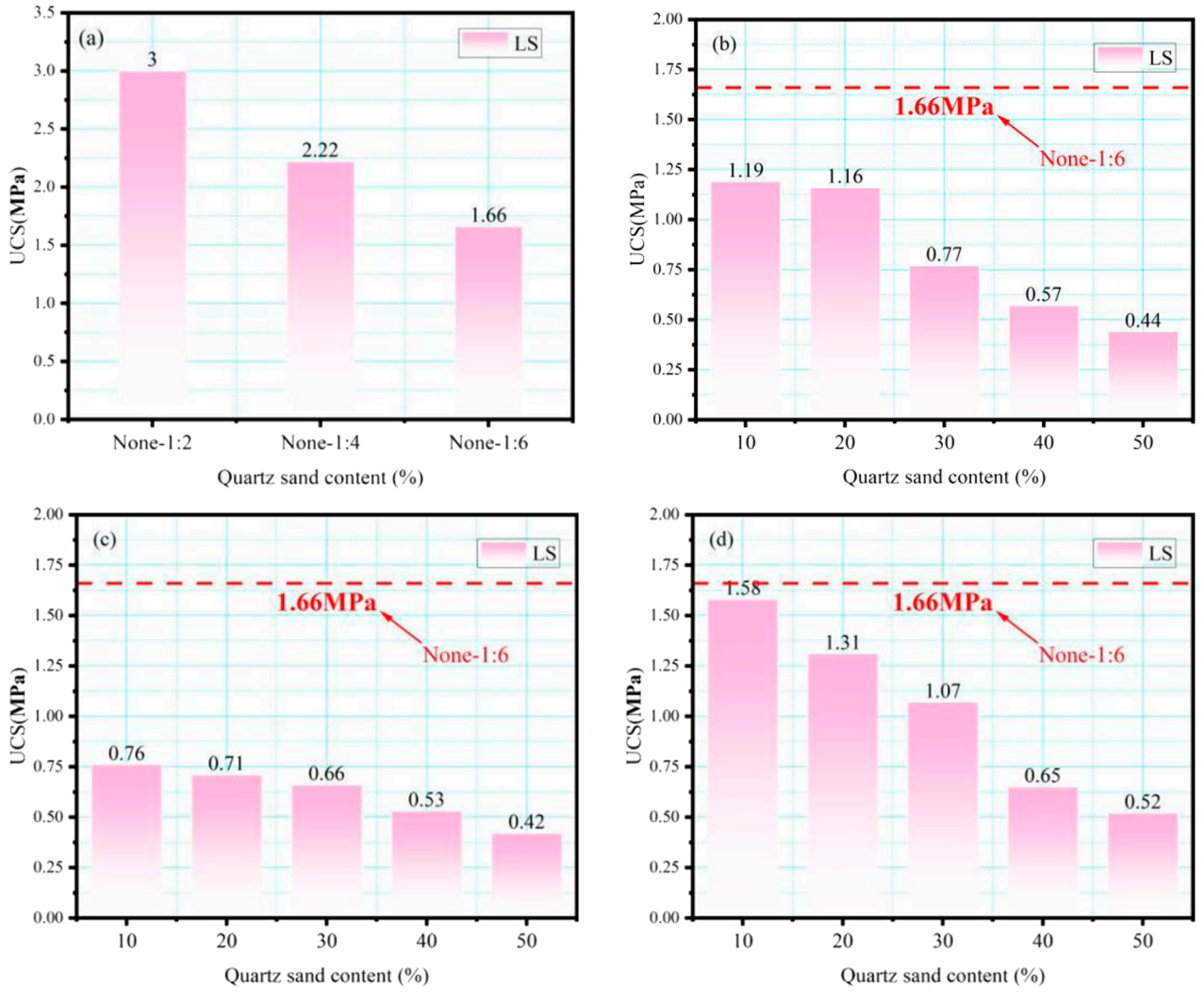

FIGURE 4
Change of packing strength under different quartz sand gradation: **(a)** control group; **(b)** 1–2 mm; **(c)** 2–4 mm; **(d)** 4–8 mm.

(Wang B. et al., 2024). Additionally, at high quartz sand contents (40%, 50%), the structural looseness became saturated, and the rate of strength reduction slowed down (Wang X. et al., 2024).

In summary, the greater the gradation of quartz sand (coarser particles), the more pronounced the decrease in backfill compressive strength. When the content is low (10%–20%), the strength decay rate accelerates, while high content (≥40%) leads to structural saturation where strength decline slows. This pattern provides a basis for blending quartz sand with different particle sizes, allowing gradation adjustments to meet various backfill strength requirements.

3.3 Evolution of the stress-strain curvature of LQCB

The stress-strain curve of the lithium slag-quartz sand cemented backfill under uniaxial loading revealed the influence of quartz sand particle size and content on the material's mechanical behavior, as shown in Figure 6. The control group (KB-1:6 (C/LS = 1:6 Lithium Slag-Quartz Sand Cemented Backfill)) contains no quartz sand. At the same time, the other specimens include different particle sizes and quartz sand contents (where "1%–2%–30%" refers to quartz sand with a particle size of 1–2 mm and a content of 30%). The deformation process can be divided into four stages: pore compression, linear elasticity, unstable rupture, and crack propagation stages, which reflect the evolution of internal structural integrity under load. 1. Pore compression stage: In the initial stage, the curve showed a slight "concave" shape, indicating the gradual closure of internal pores. Specimens with larger particle sizes (e.g., 4–8 mm) and higher contents (e.g., 50%) exhibited more pronounced compression behavior, due to the larger pores and cracks being compacted under smaller loads. The control group, which contains no quartz sand, showed weaker pore compression, indicating that the introduction of quartz sand had a significant impact on the internal structure (Zhao et al., 2022). 2. Linear elastic stage: During this stage, the curve exhibited a linear trend, indicating that the material was undergoing elastic

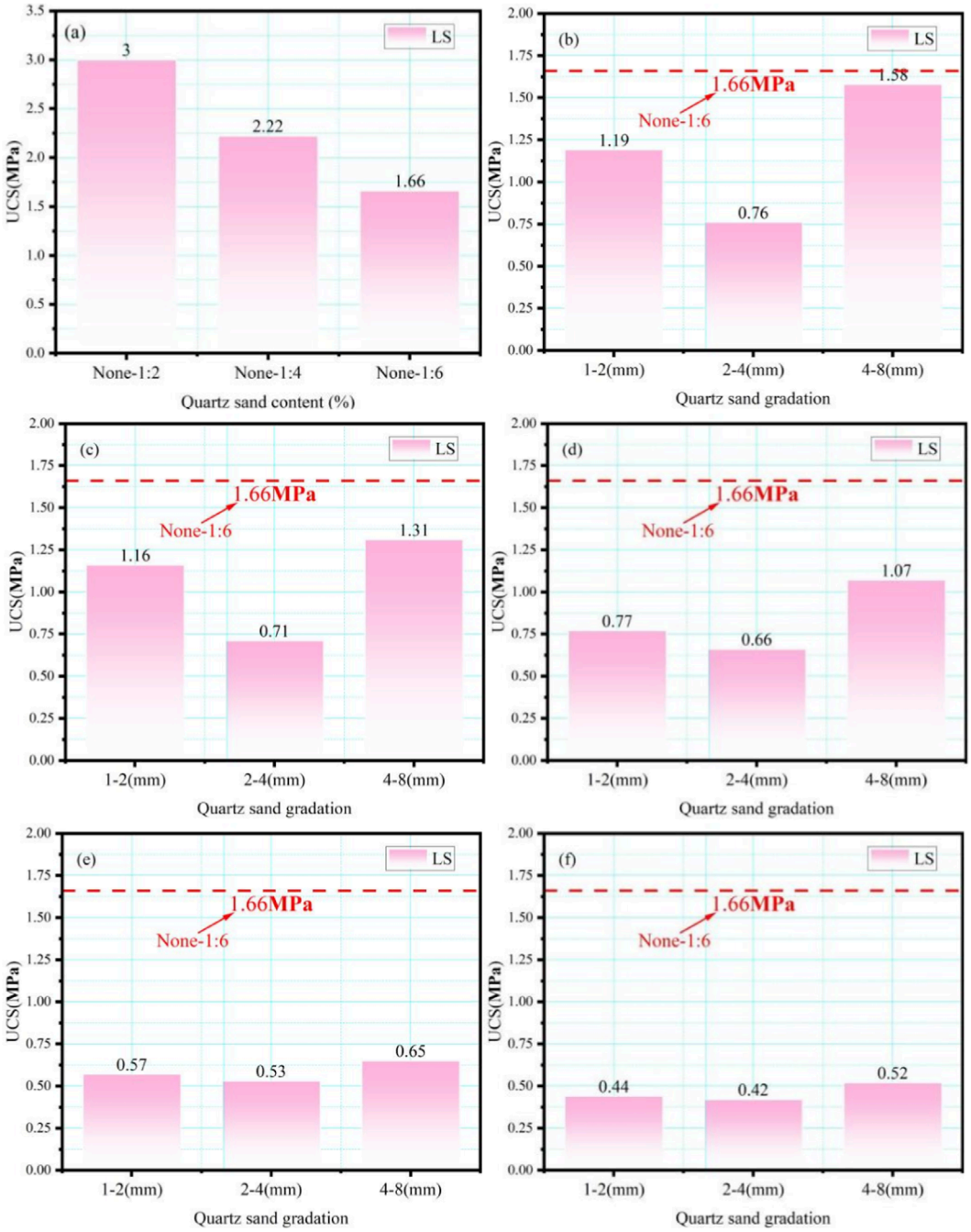

FIGURE 5
Filler strength at different quartz sand content: **(a)** 0% (control group); **(b)** 10%; **(c)** 20%; **(d)** 30%; **(e)** 40%; **(f)** 50%.

deformation. The control group reached the highest stress at this stage, suggesting that the lithium slag-based backfill without quartz sand had better cementation properties. Quartz sand with smaller particle sizes (e.g., 1–2 mm) had a larger surface area, which reduced cementation efficiency and resulted in a shorter elastic phase, whereas larger particle sizes (e.g., 4–8 mm) exhibited a longer elastic deformation (Seryakov and Krasnovsky, 2022). 3. Unstable fracture stage: In this stage, microcracks begin to form and expand, and the deformation transitions from elastic to plastic, with stress reaching its peak value. The control group exhibited the highest UCS, indicating that the lithium slag-based backfill without quartz sand had excellent mechanical properties. As the quartz sand content increased (e.g., 50%), UCS decreased significantly, indicating that excessive quartz sand dilutes the cementing matrix and weakens the internal bond strength (Hou et al., 2020). 4. Crack propagation stage: After reaching the ultimate compressive strength (UCS), the specimen entered the crack propagation stage, where stress gradually decreased as the internal structure was

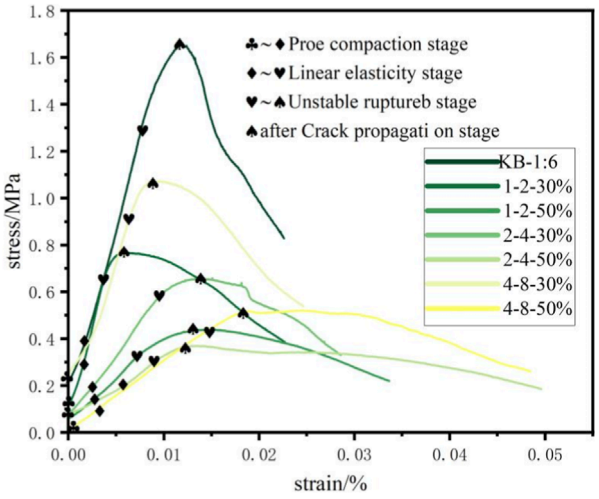

FIGURE 6
Stress-strain curvature of the LQCB specimens.

damaged. Specimens with larger particle sizes and higher contents exhibited a slower decline in stress, reflecting the locking effect of larger particles, which provided some residual strength (Qiu et al., 2018). As loading continues, cracks inside the specimen expand from micro to macro scale and gradually form a through-going main crack, ultimately leading to specimen instability and failure.

In summary, the stress-strain curve of the lithium slag-quartz sand cemented backfill exhibits four distinct phases: pore compression, linear elastic behavior, unstable fracture, and crack propagation. While large particles (4–8 mm) and high quartz sand content (50%) shorten the elastic phase and accelerate crack propagation, they provide residual strength through particle interlocking. This discovery clarifies the full-process failure mechanism of backfill materials, offering theoretical support for predicting their load-bearing capacity and deformation risks in underground mine engineering support design.

3.4 The evolution of the failure mode of LQCB

The failure modes and crack propagation behavior of LQCB specimens were significantly influenced by the water-cement ratio (w/c), quartz sand particle size, and content (Zou et al., 2024), as shown in Figure 7. Under different (w/c) ratios, the specimens primarily exhibited tensile failure modes, with the distribution and complexity of cracks being highly correlated with the (w/c) ratio. A higher (w/c) ratio (e.g., KB-1:2) led to fewer cracks with larger spacing due to excessive hydration products, showing brittle failure characteristics, while a lower (w/c) ratio (e.g., KB-1:6) resulted in more uniform crack distribution, finer cracks, enhanced ductility, and delayed formation of macro cracks (Zhao K. et al., 2023). Furthermore, the particle size and content of quartz sand also played a crucial role in determining the crack propagation behavior. Smaller particle sizes (1–2 mm) and moderate content (30%) improved the density of the structure and reduce crack complexity, while larger particle sizes (4–8 mm) and higher content (50%) increased porosity, leading to stress concentration, crack dispersion, and local failure phenomena (Chen et al., 2022; Li et al., 2021). Notably, a high quartz sand content (50%) caused brittle failure under both small and large particle size conditions, indicating that excessive quartz sand had an adverse effect on structural integrity.

In summary, backfill material failure primarily occurs through axial tensile failure. A high cement-to-lime slurry ratio (C/LS = 1:2) tends to cause brittle failure, while a lower ratio (1:6) combined with 30% quartz sand content enhances structural ductility and reduces crack formation. Conversely, excessive quartz sand (50%) regardless of particle size triggers brittle fracture. This provides an engineering solution to control failure modes through optimized mix design, effectively mitigating sudden instability risks.

3.5 Analysis of the microstructural features of LQCB

Figures 8, 9 show the SEM micrographs and EDS elemental analysis results of the "LQ-1:6" backfill specimens. From the SEM images in Figure 8, it was observed that the LQCB matrix contained a significant amount of calcium silicate hydrate (C-S-H) and ettringite (AFt). The C-S-H mixture exhibits an irregular distribution pattern, with its solid framework supported by cementitious encapsulation of quartz sand. (Zhao Y. et al., 2023), while the acicular AFt mainly filled the pores (Liu et al., 2019), thereby improving the density and volume stability of the material. The EDS analysis in Figure 9 further revealed the chemical composition of the LQCB. The main elements were calcium (34.3%), silicon (20.2%), and oxygen (28.2%), with the presence of aluminum (8.1%), sodium (4.8%), and potassium (4.4%). The Ca/Si ratio, calculated from the calcium and silicon content, was 1.7, It should be noted that unreacted silicon in quartz sand acts as an inert aggregate that does not participate in hydration reactions. Therefore, the Ca/Si ratio is used as a supplementary characterization parameter to verify the presence of C-S-H.As the primary hydration product in the backfill, the C-S-H typically appears in a flocculent form, significantly enhancing the material's density and compressive strength. Additionally, the presence of aluminum further suggested the formation of AFt, The appropriate amount of this fibrous hydration product can not only fill the pores, but also inhibit the propagation of microcracks, thus improving the volume stability and crack resistance of the material. The specimens in this study were cured for 7 days with a Ca/Si ratio of 1.7, which falls within the typical range of high-strength C-S-H (1.5–2.0). This ratio aligns with the hydration kinetics characteristics of lithium-containing slag systems, rather than being a random value. Literature have shown that higher Ca/Si ratios were typically associated with the formation of denser and more stable hydration products, significantly enhancing the compressive strength and durability of the backfill (Yu et al., 2021). It is worth noting that the specimen contains 4.8% sodium (Na) and 4.4% potassium (K). These elements likely come from the residual alkali metal minerals in the lithium slag. During hydration, these alkali metals might form soluble salts or trigger an alkali-silica reaction. However, due to their relatively

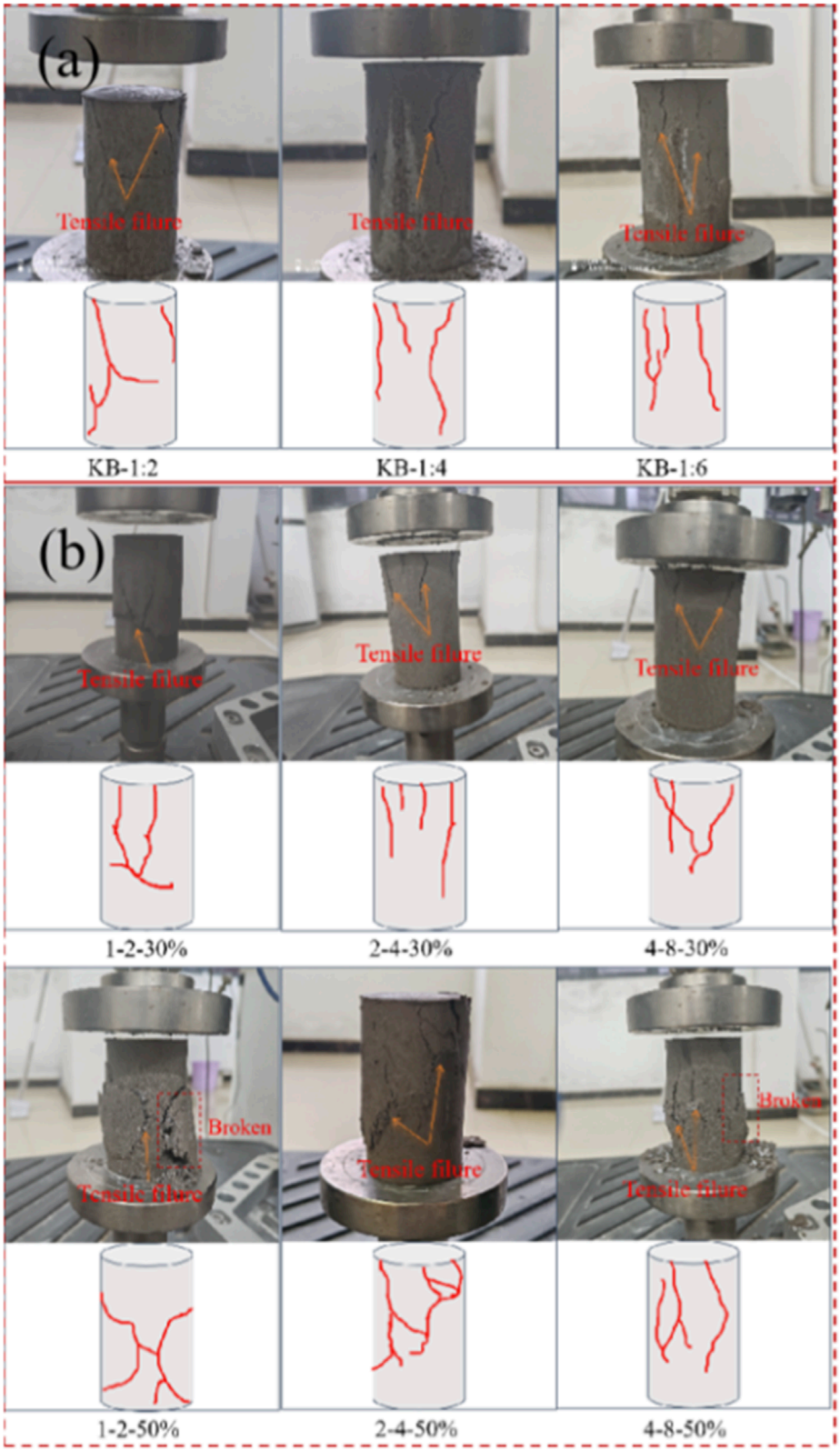

FIGURE 7
Failure mode of the specimens: **(a)** control group; **(b)** LQCB specimens.

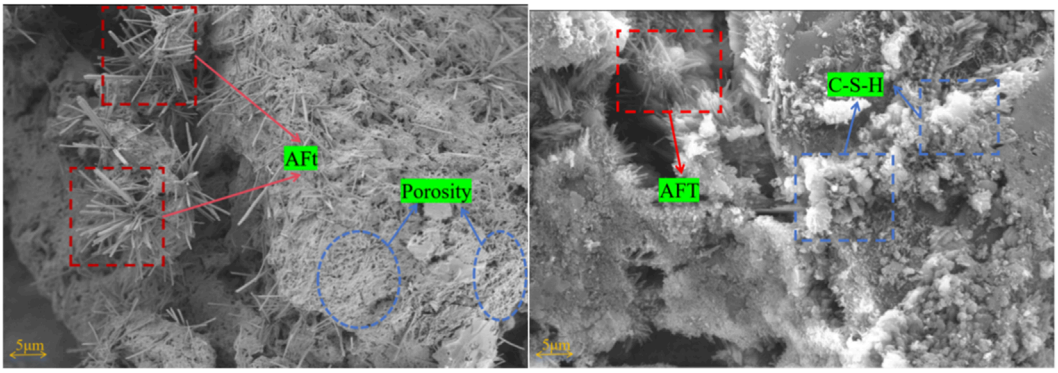

FIGURE 8
SEM analysis results of the backfill specimen prepared from lithium slag.

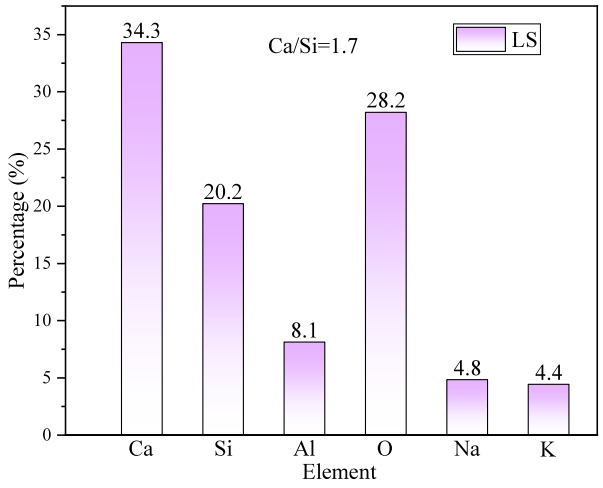

FIGURE 9
EDS values of the backfill specimen prepared from lithium slag.

low concentrations, their influence on the long-term stability of the backfill is expected to be minimal.

Figure 10 shows the SEM microstructural features of the LQCB at various proportions. As shown in Figure 10a, the hydration products were evenly distributed, and the ITZ around the quartz sand particles was dense, with small crack widths, indicating that the hydration products effectively fill the pores between the particles, significantly improving the overall compactness and mechanical properties of the backfill (Wang et al., 2020b). Figure 10b shows that when the quartz sand content increased to 50%, the hydration products were insufficiently filled, and microcracks appeared at the interface transition zone between the quartz sand particles. The crack width increased to 21 μm. This suggests that a higher aggregate proportion may lead to matrix discontinuity, thereby weakening the overall strength of the backfill (Qin et al., 2024). In Figure 10c, the crack width further increased to 40 μm. Although C-S-H and AFt were still evenly distributed on the surface of the quartz sand particles, larger microcracks persisted. This crack propagation may be related to uneven particle packing density, leading to a reduction in local structural integrity (Liu et al., 2024). Figure 10d shows that although the hydration products are distributed on both sides of the fracture, excessive particle accumulation makes it difficult for the hydration products to restrain the fracture expansion, and the fracture width increases from 40 microns to 75.6 microns, a direct increase of 25.6 microns. Figure 10e shows that the hydration products were more abundantly distributed; however, microcracks still exist, primarily concentrated at the particle-matrix interface. The crack width was smaller than the one in Figure 10d, but it still had some impact on the overall strength of the backfill. And because the particle size was too large to form a rigid skeleton, it could not directly bear the external load, resulting in increased stress. In Figure 10f, the crack width increased further to 94.7 μm, the hydration products were significantly reduced, the packing density of the quartz sand particles increased, and larger cracks were observed in the interface region. This suggests that a high aggregate proportion weakened the continuity of the matrix and the formation of hydration products (Yin et al., 2022), resulting in a significant reduction in the backfill's strength. From the comparative analysis of the SEM images and UCS data, it is evident that the microstructural features of the specimens were closely related to UCS. The larger the crack width, the lower the compressive strength. Particularly in Figure 10f, larger cracks directly led to a significant drop in strength. Moreover, the uniform distribution of hydration products (C-S-H and AFt) has a critical impact on the mechanical properties of the backfill. Despite the presence of microcracks, the even distribution of hydration products helps maintain a high UCS. However, the higher quartz sand content reduced the matrix continuity, leading to larger microcracks in the ITZ, which weakened the overall strength of the backfill.

In conclusion, the dense interface transition zone with uniform distribution of hydration products (C-S-H gel and AFt crystals) is crucial for enhancing backfill strength. Excessive quartz sand (≥50%) or coarse particles (4–8 mm) can increase crack width to a maximum of 94.7 μm, significantly degrading mechanical properties. This micro-mechanism reveals the intrinsic correlation between 'macroscopic strength and microscopic structure, providing a precise direction for optimizing backfill performance through modified hydration reactions (e.g., adding activators).

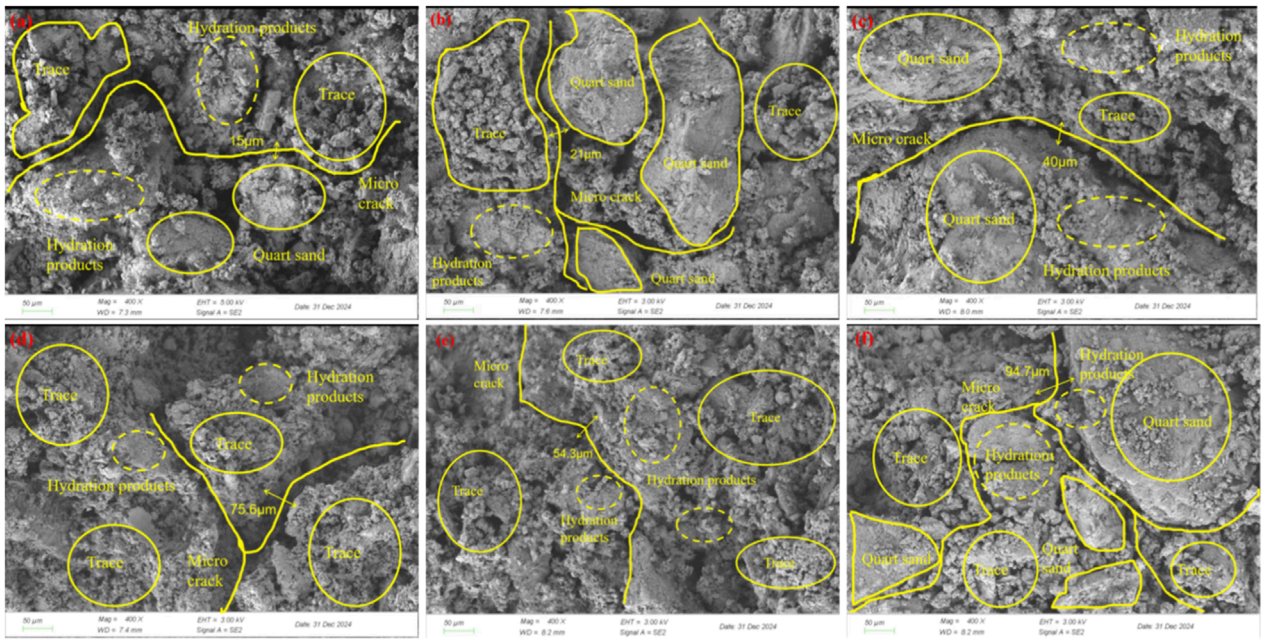

FIGURE 10
SEM micrographs of LQCB: **(a)** 1%–2%–30%; **(b)** 1%–2%–50%; **(c)** 2%–4%–30%; **(d)** 2%–4%–50%; **(e)** 4%–8%–30%; **(f)** 4%–8%–50%.

3.6 Comparison with other related studies

The study of lithium slag-quartz sand cemented backfill is of great significance in promoting the recycling of industrial waste, reducing environmental impact, and enhancing the mechanical stability of underground mining operations. Numerous studies have examined the influence of aggregate grading and particle size on the mechanical properties of cement-based backfills, thereby establishing a theoretical foundation for this research. The following is a summary of several relevant studies.

Xin (2021) evaluated the impact of waste rock content on the mechanical behavior of cemented tailings backfill through mesoscopic modeling. The study found that as the waste rock content increased, the brittleness of the backfill intensified, the compressive strength decreased, the elastic modulus increased. Crack propagation primarily concentrated in the ITZ, indicating that the proportion of waste rock in the backfill significantly affects the structural performance. Li T. et al. (2022) investigated the impact of fine aggregate gradation on the rheological properties of mortar and discovered that an optimized particle gradation can significantly enhance the packing density of aggregates and the rheological performance of the slurry, thereby improving its workability and strength. Zhang X. et al. (2023) analyzed the effect of optimized tailings gradation on the performance of cemented tailings backfill using a hydrocyclone and found that the optimal gradation yield (50%) significantly improved the compressive strength and enhanced the internal density of the backfill. Chen et al. (2023) studied the effect of nickel slag particle size on the pore structure and compressive strength of cement-based materials. The study found that optimizing particle size helps form a denser microstructure, thereby enhancing the material's mechanical properties. Wang B. et al. (2024) investigated the effect of continuous gradation on the mechanical properties of cemented tailings-waste rock backfill and found that as the gradation coefficient increased, the compressive strength showed a "first increase and then decrease" trend, which was mainly attributed to the fact that balanced gradation could improve the structural density of the backfill and reduce internal pores.

Although the aforementioned studies provide important theoretical support for optimizing the particle gradation and aggregate content of backfill materials, most of the research focuses on tailings or waste rocks, with limited studies on the combined application of lithium slag and quartz sand. Additionally, most studies only examine the effects of a single particle size or interrupted gradation, without fully addressing the role of continuous gradation in optimizing mechanical properties and microstructure. Lithium slag, as a potential active binder material, can significantly improve the cementing properties and microstructure of backfill when combined with quartz sand. Moreover, the high rigidity and low chemical reactivity of quartz sand provide potential advantages in enhancing the structural support and compressive strength of the backfill. Therefore, studying the mechanical properties and microstructure of lithium slag-quartz sand cemented backfill can not only offer new insights for the recycling of industrial solid waste but also provide theoretical support for the development of efficient mining filling technologies.

4 Conclusion

To further investigate the macro- and micro-mechanical properties of LQCB, this study conducted experiments including

UCS testing, stress-strain curve analysis, SEM microstructural examination, and EDS elemental analysis under laboratory conditions. Based on the experimental results and microstructural observations, the following main conclusions can be drawn:

1. The C/Ls ratio significantly affected the degree of hydration reaction and the formation of hydration products. When the C/Ls ratio was 1:2, more C-S-H and AFt were formed in the backfill, significantly increasing the material's density and compressive strength. As the C/Ls ratio decreased to 1:6, the hydration products decreased, and cracks in the ITZ increased, resulting in a decrease in compressive strength.
2. Quartz sand content and grading significantly affected the strength and microstructure of the backfill. When the quartz sand content was 30% and the particle size was 1–2 mm, the compressive strength of the backfill was high (0.77 MPa) and the crack width was minimum (15 μm). When the quartz sand content increased to 50%, the compressive strength decreases significantly (0.44 MPa) and the microcrack width increased (21 μ m); when the quartz sand size increased to 4–8 mm, the UCS (1.07) was 1–2 mm higher than the particle size under the skeleton effect, but the crack width increased (32.4 μm).
3. SEM images revealed that when hydration products were evenly distributed and the interface was dense, the UCS of the backfill was higher, resulting in fewer microcracks. Conversely, as the quartz sand content increased and the C/Ls ratio decreased, cracks in the interface transition zone increased in number and size, leading to a decline in mechanical properties.
4. The stress-strain curve showed typical stages of pore compaction, linear elasticity, and instability failure. The failure mode was primarily axial tensile failure, accompanied by micro-crack propagation, with cracks being more significant at higher quartz sand content.
5. The C/Ls ratio and quartz sand content significantly affected the microstructure and compressive performance of the lithium slag-quartz sand cemented backfill. When the C/Ls ratio was 1:2 and the quartz sand content was 30%, the LQCB shows better strength and stability.

This study provides a theoretical basis for optimizing the backfill ratio, thereby enhancing the mechanical properties and environmental sustainability of mine filling materials. Future research should investigate the long-term durability and field-scale performance of lithium slag-quartz sand backfill under realistic mining conditions, including the effects of chemical and mechanical weathering. Advanced characterization techniques and chemical activation methods could further optimize the material's mechanical properties and hydration mechanisms, while integration with other industrial byproducts may expand its applicability.

Data availability statement

The original contributions presented in the study are included in the article/supplementary material, further inquiries can be directed to the corresponding authors.

Author contributions

RL: Data curation, Investigation, Writing – original draft. LW: Conceptualization, Funding acquisition, Supervision, Writing – review and editing. SX: Formal Analysis, Writing – original draft. DZ: Data curation, Writing – original draft. LZ: Data curation, Software, Visualization, Writing – review and editing.

Funding

The authors declare that financial support was received for the research and/or publication of this article. The authors acknowledge financial support from the National Natural Science Foundation of China (No. 52468051).

Conflict of interest

The authors declare that the research was conducted in the absence of any commercial or financial relationships that could be construed as a potential conflict of interest.

Generative AI statement

The authors declare that no Generative AI was used in the creation of this manuscript.

Any alternative text (alt text) provided alongside figures in this article has been generated by Frontiers with the support of artificial intelligence and reasonable efforts have been made to ensure accuracy, including review by the authors wherever possible. If you identify any issues, please contact us.

Publisher's note

References

Antonovič, V., Stonys, R., Boris, R., and Malaiškienė, J. (2022). Effect of quartz sand on the properties and alkali resistance of refractory aluminosilicate castables. *Constr. Build. Mater* 351, 128978. doi:10.1016/j.conbuildmat.2022.128978

Cao, S., Xue, G., Song, W., and Teng, Q. (2020). Strain rate effect on dynamic mechanical properties and microstructure of cemented tailings composites. *Constr. Build. Mater* 247, 118537. doi:10.1016/j.conbuildmat.2020.118537

Chen, M., Wen, P., Wang, C., Chai, Z., and Gao, Z. (2020). Evaluation of particle size distribution and mechanical properties of mineral waste slag as filling material. *Constr. Build. Mater* 253, 119183. doi:10.1016/j.conbuildmat.2020.119183

Chen, G., Ye, Y., Yao, N., Fu, F., Hu, N., and Zhang, Z. (2022). Deformation failure and acoustic emission characteristics of continuous graded waste rock cemented backfill under uniaxial compression. *Environ. Sci. Pollut. Res.* 29 (53), 80109–80122. doi:10.1007/s11356-022-23394-x

Chen, S., Wang, M., Gu, L., Lin, W., Liang, J., and Korniejenko, K. (2023). Effects of incorporating large quantities of nickel slag with various particle sizes on the strength and pore structure of cement-based materials. *Constr. Build. Mater* 393, 132034. doi:10.1016/j.conbuildmat.2023.132034

Dong, L., Jiao, F., Liu, W., Wang, C., Wang, D., and Qin, W. (2024). Selective extraction of lithium and solidified fluoride from overhaul slag by the calcium sulfate roasting and water leaching. *Min. Eng.* 217, 108943. doi:10.1016/j.mineng.2024.108943

Dong, L., Jiao, F., Liu, W., and Zhang, L. (2025). Enrichment behavior of lithium enhanced by multistage water leaching of overhaul slag roasted clinker. *J. Environ. Chem. Eng.* 13 (1), 115118. doi:10.1016/j.jece.2024.115118

Guo, L., Li, W., Yang, X., and Xu, W. (2018). Sodium silicate gel effect on cemented tailing backfill that contains lead-zinc smelting slag at early ages. *Adv. Mater Sci. Eng.* 2018 (1), 8502057. doi:10.1155/2018/8502057

Hellmers, S., Qiu, H., Yagmurlu, B., and Kwade, A. (2025). Modifying milling parameters: impact on selective separation of lithium-rich phases in a thermodynamically designed battery slag. *Clean. Eng. Technol.* 24, 100857. doi:10.1016/j.clet.2024.100857

Hou, J., Guo, Z., Zhao, L., Liu, W., and Zhang, Y. (2020). Study on the damage statistical strength criterion of backfill with crack under thermo-mechanical coupling. *Int. J. Green Energy* 17 (8), 501–509. doi:10.1080/15435075.2020.1763359

Ji, G., Peng, X., Wang, S., Li, J., Sun, K., and Chi, H. (2024). Influence of ground quartz sand finesses on the formation of poorly ordered calcium silicate hydrate prepared by dynamically hydrothermal synthesis. *Case Stud. Constr. Mater* 20, e02746. doi:10.1016/j.cscm.2023.e02746

Kasap, T., Yilmaz, E., and Sari, M. (2022). Effects of mineral additives and age on microstructure evolution and durability properties of sand-reinforced cementitious mine backfills. *Constr. Build. Mater* 352, 129079. doi:10.1016/j.conbuildmat.2022.129079

Kolandhasamy, P., Elumalai, S., Nandagopal, S., Senthil Kumaran, S., Rajendran, R., Vinayagam, R., et al. (2024). A preliminary health risk assessment of heavy metal contamination in Chembarambakkam Lake, Tamil Nadu, South India. *Water* 16, 3517. doi:10.3390/w16233517

Li, T., Zhou, Y., Zhu, J., and Liu, J. (2022). Effect of fine aggregate gradation on the rheology of mortar. *Constr. Build. Mater* 332, 127362. doi:10.1016/j.conbuildmat.2022.127362

Li, X., Tao, Z., Wang, J., Zuo, T., Ma, J., and Li, Q. (2021). Strain rate effect on mechanical properties of cemented backfill under dynamic and static combined loading. *Shock Vib.* 2021 (1), 2196838. doi:10.1155/2021/2196838

Li, M., Zhang, J., Guo, Y., Pu, H., and Peng, Y. (2022). Influence of particle size distribution on fractal characteristics of waste rock backfill materials under compression. *J. Mater Res. Technol.* 20, 2977–2989. doi:10.1016/j.jmrt.2022.08.056

Li, N., Yu, S., Wu, E., Song, X., Jiang, P., Xu, H., et al. (2024). Study on small strain characteristics and microscopic mechanism of rice husk ash modified lime soil. *Transp. Geotech.* 45, 101209. doi:10.1016/j.trgeo.2024.101209

Li, H., Jin, A., Chen, S., and Zhao, Y. (2024). Mechanical properties and microstructure of coal cinder-based ultra-fine tailings cemented tailings body. *Case Stud. Constr. Mater* 20, e02763. doi:10.1016/j.cscm.2023.e02763

Liu, L., Cai, G., Liu, X., Liu, S., and Puppala, A. J. (2019). Evaluation of thermal-mechanical properties of quartz sand-bentonite-carbon fiber mixtures as the borehole backfilling material in ground source heat pump. *Energy Build.* 202, 109407. doi:10.1016/j.enbuild.2019.109407

Liu, W., Yu, H., Wang, S., Wei, M., Wang, X., Tao, T., et al. (2023). Evolution mechanism of mechanical properties of cemented tailings backfill with partial replacement of cement by rice straw ash at different binder content. *Powder Technol.* 419, 118344. doi:10.1016/j.powtec.2023.118344

Liu, Y., Deng, H., Jiang, Z., Tian, G., Wang, P., and Yu, S. (2024). Research on influence laws of aggregate sizes on pore structures and mechanical characteristics of cement mortar. *Constr. Build. Mater* 442, 137606. doi:10.1016/j.conbuildmat.2024.137606

Lu, Q., Jiang, Z., Tang, P., Yu, C., Jiang, F., Huang, J., et al. (2023). Identify the potential driving mechanism of reconstructed bacterial community in reduce CO2 emissions and promote humus formation during cow manure composting. *J. Environ. Manage* 345, 118896. doi:10.1016/j.jenvman.2023.118896

Lyu, H., Chen, Y., Pu, H., Ju, F., Zhang, K., Li, Q., et al. (2023). Dynamic properties and fragmentation mechanism of cemented tailings backfill with various particle size distributions of aggregates. *Constr. Build. Mater* 366, 130084. doi:10.1016/j.conbuildmat.2022.130084

Ma, Y., Sheng, J., Li, T., Yang, C., Xiao, Q., and Yang, R. (2023). Study on the optimal conditions of ultrasonic strengthening phosphogypsum storage and solidification of CO2. *Sustain Chem. Pharm.* 33, 101091. doi:10.1016/j.scp.2023.101091

Nongthombam, G. S., Saikia, A., and Borah, J. C. (2024). The chronological evolution of environment benign processes in the synthesis of natural products and APIs. *Sustain Chem. Pharm.* 41, 101725. doi:10.1016/j.scp.2024.101725

Qin, H., Cao, S., and Yilmaz, E. (2024). Mechanical, energy evolution, damage and microstructural behavior of cemented tailings-rock fill considering rock content and size effects. *Constr. Build. Mater* 411, 134449. doi:10.1016/j.conbuildmat.2023.134449

Qiu, J., Yang, L., Xing, J., and Sun, X. (2018). Analytical solution for determining the required strength of mine backfill based on its damage constitutive model. *Soil Mech. Found. Eng.* 54 (6), 371–376. doi:10.1007/s11204-018-9483-7

Sari, M., Yilmaz, E., and Kasap, T. (2023). Long-term ageing characteristics of cemented paste backfill: usability of sand as a partial substitute of hazardous tailings. *J. Clean. Prod.* 401, 136723. doi:10.1016/j.jclepro.2023.136723

Seryakov, V. M., and Krasnovsky, A. A. (2022). Stress–strain behavior of rock mass around the roadway with roof support of rock fall-hazardous zones by the phenolic resin fill. *IOP Conf. Ser. Earth Environ. Sci.* 991 (1), 012002. doi:10.1088/1755-1315/991/1/012002

Shi, Y., Cheng, L., Tao, M., Tong, S., Yao, X., and Liu, Y. (2020). Using modified quartz sand for phosphate pollution control in cemented phosphogypsum (PG) backfill. *J. Clean. Prod.* 283, 124652. doi:10.1016/j.jclepro.2020.124652

Song, X., Hao, Y., Wang, S., Zhang, L., Liu, W., and Li, J. (2022). Mechanical properties, crack evolution and damage characteristics of prefabricated fractured cemented paste backfill under uniaxial compression. *Constr. Build. Mater* 330, 127251. doi:10.1016/j.conbuildmat.2022.127251

Stukhlyak, P. D., Buketov, A. V., Panin, S. V., Maruschak, P. O., Moroz, K. M., Poltaranin, M. A., et al. (2015). Structural fracture scales in shock-loaded epoxy composites. *Phys. Mesomech.* 18 (1) 58–74. doi:10.1134/S1029959915010075

Wang, J., Fu, J., Song, W., Zhang, Y., and Wang, Y. (2020a). Mechanical behavior, acoustic emission properties and damage evolution of cemented paste backfill considering structural feature. *Constr. Build. Mater* 261, 119958. doi:10.1016/j.conbuildmat.2020.119958

Wang, J., Guo, Y., and Shang, J. Q. (2020b). Portland cement stabilisation of Canadian mature fine oil sands tailings. *Environ. Geotech.* 10 (6), 380–389. doi:10.1680/jenge.19.00158

Wang, Y., Wu, J., Ma, D., Yang, S., Yin, Q., and Feng, Y. (2022). Effect of aggregate size distribution and confining pressure on mechanical property and microstructure of cemented gangue backfill materials. *Adv. Powder Technol.* 33 (8), 103686. doi:10.1016/j.apt.2022.103686

Wang, J., Zhang, C., Song, W., and Zhang, Y. (2022). The energy dissipation, AE characteristics, and microcrack evolution of rock–backfill composite materials (RBCM). *Minerals* 12 (4), 482. doi:10.3390/min12040482

Wang, B., Kang, M., Liu, C., Yang, L., Li, Q., and Zhou, S. (2024). Experimental study on mechanical and microstructure properties of cemented tailings-waste rock backfill with continuous gradation. *J. Build. Eng.* 95, 110146. doi:10.1016/j.jobe.2024.110146

Wang, X., Guo, J., Wu, A., Wang, H., Jiang, H., Li, Z., et al. (2024). Wear characteristics of the pipeline transporting cemented paste backfill containing coarse aggregate. *Constr. Build. Mater* 410, 134170. doi:10.1016/j.conbuildmat.2023.134170

Wei, H., Shan, X., Wu, L., Zhang, J., Saleem, M., Yang, J., et al. (2023). Microbial cell membrane properties and intracellular metabolism regulate individual level microbial responses to acid stress. *Soil Biol. Biochem.* 177, 108883. doi:10.1016/j.soilbio.2022.108883

Wu, L., Mu, B., Yang, H., Zhao, F., Zhu, Y., and Wang, A. (2022). Fabrication of multifunctional carbon/clay nanocomposites by recycling oil shale semi-coke waste for coloring and enhancing mechanical and aging-resistant properties of acrylonitrile–butadiene–styrene. *Mater Today Sustain* 20, 100259. doi:10.1016/j.mtsust.2022.100259

Xin, L. (2021). Meso-scale modeling of the influence of waste rock content on mechanical behavior of cemented tailings backfill. *Constr. Build. Mater* 307, 124473.doi:10.1016/j.conbuildmat.2021.124473

Xin, J., Liu, L., Xu, L., Wang, J., Yang, P., and Qu, H. (2022). A preliminary study of aeolian sand-cement-modified gasification slag-paste backfill: fluidity, microstructure, and leaching risks. *Sci. Total Environ.* 830, 154766. doi:10.1016/j.scitotenv.2022.154766

Yang, X., Tu, B., Wu, S., Xu, S., Song, Y., Chen, D., et al. (2025). Performance evaluation of pre-stressed high-strength concrete pipe piles produced with steel slag powder and ground quartz sand as composite supplementary cementitious materials. *Constr. Build. Mater* 478, 141451. doi:10.1016/j.conbuildmat.2025.141451

Yin, S., Zhou, Y., Wang, L., Pan, J., and Kou, Y. (2022). Setting, bleeding, and hardening strength properties of coarse aggregate backfill slurry. *Case Stud. Constr. Mater* 17, e01667. doi:10.1016/j.cscm.2022.e01667

Yu, X., Kemeny, J., Tan, Y., Song, W., and Huang, K. (2021). Mechanical properties and fracturing of rock-backfill composite specimens under triaxial compression. *Constr. Build. Mater* 304, 124577. doi:10.1016/j.conbuildmat.2021.124577

Yuan, L., Liu, L., Sun, L., Liu, Q., Li, M., and Liu, N. (2024). Feasibility study of lithium slag as cementitious material with high-content application in cement stabilized macadam bases. *Constr. Build. Mater* 457, 139224. doi:10.1016/j.conbuildmat.2024.139224

Zhang, H., Cao, S., and Yilmaz, E. (2023). Influence of 3D-printed polymer structures on dynamic splitting and crack propagation behavior of cementitious tailings backfill. *Constr. Build. Mater* 343, 128137. doi:10.1016/j.conbuildmat.2022.128137

Zhang, X., Wu, D., Lu, H., Liu, L., and Zheng, S. (2023). Improvement of tailings gradation on workability and strength of cemented tailings backfill. *Constr. Build. Mater* 387, 131633. doi:10.1016/j.conbuildmat.2023.131633

Zhao, K., He, Z., Yang, J., Yan, Y., Zhao, X., Liu, L., et al. (2022). Damage constitutive modeling of backfills with different cement–tailing ratios using energy method. *Geotech. Geol. Eng.* 41 (2), 1005–1017. doi:10.1007/s10706-022-02319-y

Zhao, K., Yang, J., Yu, X., Yan, Y., Zhao, K., Lai, Y., et al. (2023). Damage evolution process of fiber-reinforced backfill based on acoustic emission three-dimensional localization. *Compos Struct.* 309, 116723. doi:10.1016/j.compstruct.2023.116723

Zhao, Y., Zhao, G., Xu, L., Zhou, J., and Huang, X. (2023). Mechanical property evolution model of cemented tailings-rock backfill considering strengthening and weakening effects. *Constr. Build. Mater* 377, 131081. doi:10.1016/j.conbuildmat.2023.131081

Zhou, N., Zhang, J., Ouyang, S., Deng, X., Dong, C., and Du, E. (2020). Feasibility study and performance optimization of sand-based cemented paste backfill materials. *J. Clean. Prod.* 259, 120798. doi:10.1016/j.jclepro.2020.120798

Zhu, X., Zhang, W., Wang, Y., Lv, W., and Ma, C. (2023). Diffusion mechanism of solid waste product utilization pulping and fracture network grouting. *Constr. Build. Mater* 408, 133571. doi:10.1016/j.conbuildmat.2023.133571

Zhu, T., Chen, Z., Wang, Z., Cao, J., Hao, J., and Zhou, Z. (2025). Energy damage evolution and mesoscopic failure mechanism of cemented waste rock tailing backfill under axial compression. *Structures* 71, 108057. doi:10.1016/j.istruc.2024.108057

Zou, S., Cao, S., and Yilmaz, E. (2024). Effect of content of defluorinated solid waste on macroscopic strength and microstructural evolution of cemented tail filling composites. *Constr. Build. Mater* 436, 136921. doi:10.1016/j.conbuildmat.2024.136921